

CPAC-Conv: CP-decomposition to Approximately Compress Convolutional Layers in Deep Learning

Yinan Wang¹, Weihong (Grace) Guo², and Xiaowei Yue^{1*}

¹Virginia Tech, Blacksburg, VA, 24061

²Rutgers University, New Brunswick, NJ, 08901

ARTICLE HISTORY

Compiled May 29, 2020

ABSTRACT

Feature extraction for tensor data serves as an important step in many tasks such as anomaly detection, process monitoring, image classification, and quality control. Although many methods have been proposed for tensor feature extraction, there are still two challenges that need to be addressed: 1) how to reduce the computation cost for high dimensional and large volume tensor data; 2) how to interpret the output features and evaluate their significance. Although the most recent methods in deep learning, such as Convolutional Neural Network (CNN), have shown outstanding performance in analyzing tensor data, their wide adoption is still hindered by model complexity and lack of interpretability. To fill this research gap, we propose to use CP-decomposition to approximately compress the convolutional layer (CPAC-Conv layer) in deep learning. The contributions of our work could be summarized into three aspects: 1) we adapt CP-decomposition to compress convolutional kernels and derive the expressions of both forward and backward propagations for our proposed CPAC-Conv layer; 2) compared with the original convolutional layer, the proposed CPAC-Conv layer can reduce the number of parameters without decaying prediction performance. It can combine with other layers to build novel Neural Networks; 3) the value of decomposed kernels indicates the significance of the corresponding feature map, which increases model interpretability and provides us insights to guide feature selection.

*corresponding author: Dr. Xiaowei Yue. Email: xwy@vt.edu

KEYWORDS

CP-decomposition, Tensor, Convolutional Neural Network (CNN), Model compression, Feature extraction

1. Introduction

With the development of sensing technology in recent years, the high-rate and high-resolution image sensors have become ubiquitous in the smart manufacturing systems. Compared with other data types, i.e. spectrum, vector, etc., image data is more straightforward and easy to understand by human eyes. Images could convey rich and various information associated with 2D or 3D geometries, spatial-temporal structures, and multi-channel dynamic changes. Therefore, they are becoming more and more critical in many applications such as anomaly detection (Yan et al., 2017), spatiotemporal characterization (Shao et al., 2017), quality prediction (Li et al., 2020), high dimensional profile monitoring (Sergin and Yan, 2019), quality control and process optimization (Gao et al., 2020, Liu et al., 2019).

In the pipeline of image-based data analysis, feature extraction is one essential intermediate step. Most of the applications are implemented based on specific features. Deterministic and stochastic decompositions are effective ways to learn informative features (Yue, 2019). For example, Principal component analysis (PCA) and its variants are classical feature extraction techniques designed for learning a lower-dimensional representation of the original data. Since traditional PCA is mainly applicable for vectors or matrices, while the color images are 3-way tensors (multi-arrays), Unfolded PCA (UPCA) is proposed to unfold the multi-way tensors into matrix or vectors and then extract the principal components (Nomikos and MacGregor, 1994). However, UPCA could destroy the structure and spatial information of multi-way tensors. To tackle this issue, Tensor-based PCA was proposed to bridge the gap between traditional PCA and multi-way tensors (Vasilescu and Terzopoulos, 2002), which could directly learn the representation of a multi-way tensor without changing its structure. Generalized PCA (GPCA) was proposed to consider the spatial locality of pixels in 2D images (Ye et al., 2004), which could extract features by projecting the 2D images into a vector space. Multi-linear PCA (MPCA) and Uncorrelated multi-linear PCA

(UMPCA) were proposed to find the orthogonal basis to capture the most of variation in the original multi-way tensor and avoid the correlations among features (Lu et al., 2008). Although the PCA methods can compress data and extract features in a simple and scalable way, their effectiveness is hindered by the high computational cost when applied to high-dimensional tensors, the assumption that the original data is the linear combination of principal components, and the interpretability of principal components. To specify the meaning of each decomposed components, Smooth-sparse Decomposition (SSD) was proposed to decompose an image into three components, which are smooth background, sparse anomalous regions, and the random noise (Yan et al., 2017). This decomposition achieved excellent performance in anomaly detection for images.

Apart from PCA related methods, tensor decomposition techniques can also be used for feature extraction. The CANDECOMP/PARAFAC (CP) decomposition (Kiers, 2000) can approximate the original tensor with the summation of rank-one tensors, and Tucker decomposition (Tucker, 1966c) can decompose the original tensor into a core tensor along with multiple matrices. Kolda and Bader (2009) and Papalexakis et al. (2016) did thorough literature reviews about tensor decomposition. Yue et al. (2020) proposed a tensor mixed effects model to decompose fixed effects and random effects in tensors and learn correlations along different dimensions. Gao et al. (2020) integrated tensor decomposition and ensemble learning by utilizing the mutual benefits so as to improve quality evaluation.

The aforementioned feature extraction techniques are mainly derived from the perspective of statistics. Some mathematical signal processing techniques (specifically computational harmonic analysis) can be used to extract features from image data. In the field of signal processing, transformation methods will transform an image into a new domain based on the spatial frequencies characteristics of the pixel intensity variations. Multi-way PCA (MPCA) and 2D Fast Fourier Transformation (FFT) have been applied to extract texture features from images (Geladi, 1992). Wavelet transformation also showed its advantages in signal decomposition and has the potential to extend to multi-way tensor (Mallat, 1989). Jin and Shi (1999) firstly proposed wavelet-based profile monitoring for quality control. Wavelet-based feature extraction

was further been adapted to profile data and multi-channel profile data for real-time detection and quality improvement in advanced manufacturing systems (Paynabar and Jin, 2011, Yue et al., 2018).

Recently developed deep learning methods have become another important branch in feature extraction techniques. Among all the structures of neural networks, Convolutional Neural Network (CNN) is designed to process multi-way tensor data and has shown its strength in many fields such as object detection, classification, segmentation, etc. ImageNet was the first CNN model proposed for classification tasks and outperformed the previous methods (Krizhevsky et al., 2012). In the structure of ImageNet, the Convolutional layer (Conv layer) acts as the feature extractor and the Fully Connected layer (FC layer) acts as the classifier. Various works on designing novel CNN structures follow a similar idea, that is to design multiple Convolutional layers as the feature extractor, and use other types of layers according to the specific tasks (Girshick, 2015, He et al., 2016, Simonyan and Zisserman, 2015). The aforementioned models are supervised methods, which means all the features from images are extracted on the guidance of specific tasks. Auto-encoder is a family of unsupervised learning methods focusing on extracting features from multi-way tensors. Stacked Convolutional Auto-Encoders (CAE) was proposed for unsupervised hierarchical feature extraction (Masci et al., 2011). Recently, deep probabilistic autoencoders are proposed for high-dimensional profile monitoring in the field of manufacturing systems (Sergin and Yan, 2019).

Although deep learning has shown its strength in processing high dimensional and large-volume data, the model complexity and computational cost are still significant and hard to adapt the models to devices with limited computational resources. Additionally, large parameter size makes features from the deep learning methods hard to interpret. Recently, more and more research works focus on compressing deep learning models as well as maintaining their performance. Given the fact that most of the trainable weights in Neural Network are in the tensor format and the operations in Neural Network can also be expressed as tensor operations, some research works tried to apply tensor decomposition techniques to project the weight tensors into a lower dimension space. For the weight tensor of the fully-connected layers (FC layers), a

Tensor Train format (TT-format) was proposed to represent the weight tensor as the product of a series of lower-dimensional matrices (Novikov et al., 2015). Tucker Tensor Layer (TTL) was proposed to employ Tucker Decomposition to decompose the weight tensor of FC layers into a core tensor and factor matrices (Calvi et al., 2019). The main idea of these works is to approximate the high-dimensional weight tensor by using lower-dimensional matrices with fewer parameters and then to derive the gradients with respect to (w.r.t.) the decomposed components for parameter update. It is relatively straightforward to substitute decomposed components into expressions of FC layers. Since the Convolutional layer (Conv layer) of CNN may generate a large number of unknown parameters especially in very deep CNN models. CP-decomposition can be applied to decompose the weight tensor in the Conv layer to reduce the number of parameters (Lebedev et al., 2015). The idea is to train the CNN model at first, and decompose the weight tensor, finally finetune the decomposed weights on the training data. However, this indirect training method will introduce extra computation cost in the training phase. Because there is no derivation of gradients w.r.t. the decomposed weights, it is impossible to train the decomposed weights from scratch directly.

In this paper, we propose a novel layer to use CP-decomposition to approximately compress the Convolutional layer (CPAC-Conv layer). We derive the expressions of both forward and backward propagation according to the first principles and matrix calculus. First, we derive the tensor expression of the Conv layer. Next, substitute the CP-decomposition results of weight tensor into original expression and formulate the forward propagation expression of the CPAC-Conv layer. To make our model learn the unknown parameters efficiently, we further derive the gradients w.r.t. each decomposed weight matrices to complete the backward propagation. To the best of our knowledge, our work is the first attempt to approximate and compress the Convolutional layer and derive the complete expressions of both the forward and backward propagations. The contributions of this paper could be summarized as three aspects: 1) it creates a novel CPAC-Conv layer and derives the forward and backward propagation of proposed CPAC-Conv layer; 2) the proposed CPAC-Conv layer uses fewer parameters to realize the comparable performance with original Convolutional layers in deep learning models; 3) the CPAC-Conv layer provides an alternative way to interpret the extracted

features.

The remainder of the paper will be organized as follows. Section 2 introduces the theoretical backgrounds needed for method derivation, which include CP-decomposition and matrix calculus; Section 3 creates the CPAC-Conv layer and contains the complete derivation of forward and backward propagation of CPAC-Conv layer; Section 4 introduces how to build up new Convolutional Neural Network with CPAC-Conv layers (CPAC-CNN) and generates the training algorithm of CPAC-CNN; Section 5 shows the model performance on classification task using MNIST dataset (LeCun and Cortes, 2010) and Magnetic Tile Defect dataset (Huang et al., 2018) and justifies the contributions of our work; Section 6 summarizes the conclusion of this paper.

2. Theoretical Backgrounds

Before diving into the detailed introduction of the CP-decomposed Convolutional layer, we first introduce the necessary theoretical backgrounds needed to derive and propose our method.

2.1. CP-Decomposition

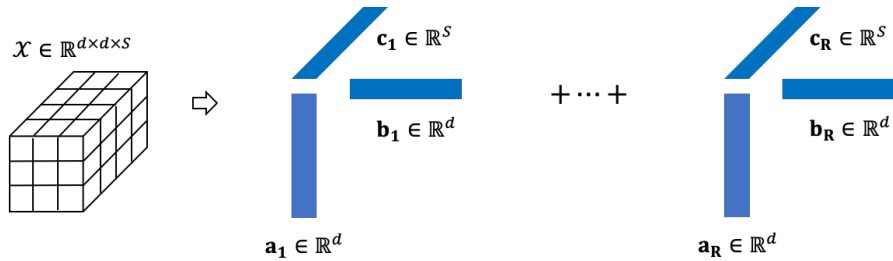


Figure 1. CP-decomposition of three-way tensor \mathcal{X}

The CANDECOMP/PARAFAC (CP) decomposition decomposes a tensor into a sum of rank-one tensors (Lebedev et al., 2015). For example, as shown in Figure 1, a three-way tensor $\mathcal{X} \in \mathbb{R}^{d \times d \times S}$ can be decomposed into the summation of $a_i \in \mathbb{R}^d, b_i \in \mathbb{R}^d, c_i \in \mathbb{R}^S, i = 1, \dots, R$. The expression of CP-decomposition is given as below, where

the operator \circ represents outer product.

$$\mathcal{X} \approx \sum_{i=1}^R \mathbf{a}_i \circ \mathbf{b}_i \circ \mathbf{c}_i \quad (1)$$

Based on the CP-decomposition on three-way tensor, it can be further extended to a general N_{th} -order tensor, $\mathcal{X} \in \mathbb{R}^{I_1 \times I_2 \times \dots \times I_N}$. The expression of general CP-decomposition is given as equation (2), where the λ_r represents the weights of each rank.

$$\mathcal{X} \approx \sum_{i=1}^R \lambda_r \mathbf{a}_i^{(1)} \circ \mathbf{a}_i^{(2)} \circ \dots \circ \mathbf{a}_i^{(N)} \quad (2)$$

CP-decomposition is one of the most popular tensor decompositions due to its intuitive interpretation and its uniqueness under very mild conditions. Practically, the uniqueness of extracted features indicates that the CP decomposition may uncover the latent factors and hidden patterns.

2.2. Matrix Calculus

Matrix calculus is an important prerequisite in our proposed method. At first, the column stacking vectorization of a matrix $X \in \mathbb{R}^{m \times n}$ is given as equations (3) (Fackler, 2005).

$$\text{vec}(X) = [X_{11}, \dots, X_{m1}, X_{12}, \dots, X_{m2}, \dots, X_{1n}, \dots, X_{mn}]^T \in \mathbb{R}^{mn \times 1} \quad (3)$$

And then, there is an important relationship between the Kronecker product and the vectorization.

Lemma 2.1 ((Magnus and Neudecker, 1985)). *For any three matrices A, X, B , such that the matrix product AXB is defined,*

$$\text{vec}(AXB) = (B^T \otimes A)\text{vec}(X) \quad (4)$$

Furthermore, matrix derivative is essential in deriving back-propagation expressions of our proposed CPAC-Conv layer. Suppose we have matrix $F \in \mathbb{R}^{p \times q}$ and $X \in \mathbb{R}^{m \times n}$, we define the derivative of F w.r.t. X as equation (5).

Definition 2.2 ((Magnus and Neudecker, 1985)). Let F be a differentiable $p \times q$ real matrix function of an $m \times n$ matrix of real variables X . The derivative of F at X is the $mn \times pq$ matrix.

$$\frac{\partial F}{\partial X} = \frac{\partial \text{vec}(F)}{\partial \text{vec}(X)} \quad (5)$$

We also have the extension of the first identification theorem, which describes the relationship between the vectorized matrix differential and derivative shown in equation (6) (Crowder et al., 1989).

$$\text{vec}(dF) = \frac{\partial F^T}{\partial X} \text{vec}(dX) \quad (6)$$

3. Adapt CP-decomposition to Approximately Compress Convolutional Layer

In this section, we will create a novel CPAC-Conv layer by adapting CP-decomposition to approximately compress the convolutional layer. In general, the basic ideas of our proposed CPAC-Conv layer could be summarized into three aspects: (a) Since the high-rank tensor could be approximated by the summation of rank-one tensors, we could reduce the parameters in convolution layer by replacing the convolution kernel with a group of rank-one kernels given by CP-decomposition; (b) Since the accuracy of CP-decomposition could be controlled by the hyper-parameter R shown in equation (2),

our proposed method still maintains the potential to further improve its performance by tuning R ; (c) Convolution operations over those decomposed rank-one kernels can be regarded as a sequence of convolution operations along each axis of the input tensor. In this section, we will derive the expressions of forward and backward propagations of the CPAC-Conv layer, which provides theoretical support to build and train new Deep Neural Networks with one or more CPAC-Conv layers.

3.1. Expression of Convolutional Operation

At first, we need to develop the expression of the original convolutional operation. Suppose the input tensor of a convolutional layer is $\mathcal{U} \in \mathbb{R}^{X \times Y \times S}$, in which X, Y represent width and height respectively and S represents the number of channels. The convolution kernel is $\mathcal{K} \in \mathbb{R}^{d \times d \times S \times N}$, in which d is the kernel size, S is the number of input channels, and N is the number of output channels. Given the stride is one and no padding applied, the output tensor should be $\mathcal{V} \in \mathbb{R}^{(X-\Delta) \times (Y-\Delta) \times N}$, in which $\Delta = d - 1$, and 1 is determined by stride. The scalar expression of convolutional operation is given by equation (7).

$$\mathcal{V}(x, y, n) = \sum_{i=x}^{x+d-1} \sum_{j=y}^{y+d-1} \sum_{s=1}^S \mathcal{K}(i-x, j-y, s, n) \mathcal{U}(i, j, s) \quad (7)$$

Based on the equation (7), in the following sections, we will derive the expressions of forward and backward propagation of CPAC-Conv layer by adapting CP-decomposition to original convolution operation.

3.2. Forward Propagation of CPAC-Conv Layer

To formulate the forward propagation of CPAC-Conv layer, we need at first apply CP-decomposition on the original convolutional kernel \mathcal{K} , which is a 4-way tensor with the shape of $d \times d \times S \times N$. The CP-decomposition of kernel \mathcal{K} is given as equation

(8).

$$\mathcal{K} = \sum_{r=1}^R K_r^X \circ K_r^Y \circ K_r^S \circ K_r^N \quad (8)$$

In equation (8), the decomposed rank-one tensors, $K_r^X, K_r^Y, K_r^S, K_r^N, r = 1, \dots, R$, could be regarded as the group of small kernels. We can approximate the original convolution operation by a sequence of convolution operations with smaller kernels along each axis of input tensor and the channels of output. After substituting the equation (8) into equation (7), the scalar expression of forward propagation can be obtained (Lebedev et al., 2015), as shown in equation (9).

$$\mathcal{V}(x, y, n) = \sum_{r=1}^R K_r^N(n) \left(\sum_{i=x}^{x+d-1} K_r^X(i-x) \left(\sum_{j=y}^{y+d-1} K_r^Y(j-y) \left(\sum_{s=1}^S K_r^S(s) \mathcal{U}(i, j, s) \right) \right) \right) \quad (9)$$

Next, we need to further reformulate the scalar expression (9) into tensor expression. At first, we reshape the input $\mathcal{U} \in \mathbb{R}^{X \times Y \times S}$ into $\tilde{\mathcal{U}} \in \mathbb{R}^{d \times d \times S \times (X-d+1)(Y-d+1)}$. The Figure 2 shows an example of reshaping with $d = 3$. Intuitively, as the original convolution operation is implemented by sliding the convolution kernel over the input tensor, the reshape process will duplicate and reorganize the input tensor to enable convolution operation finished by tensor production. The corresponding tensor expression of equation (9) is shown in equation (10).

$$\tilde{\mathcal{V}} = \sum_{r=1}^R \left(\left(\left(\tilde{\mathcal{U}} \times_3 K_r^S \right) \times_2 K_r^Y \right) \times_1 K_r^X \right) \circ K_r^N \quad (10)$$

The output $\tilde{\mathcal{V}}$ is of shape $(X-d+1)(Y-d+1) \times N$, which can be transformed into the output of equation (7) by one more step of reshaping.

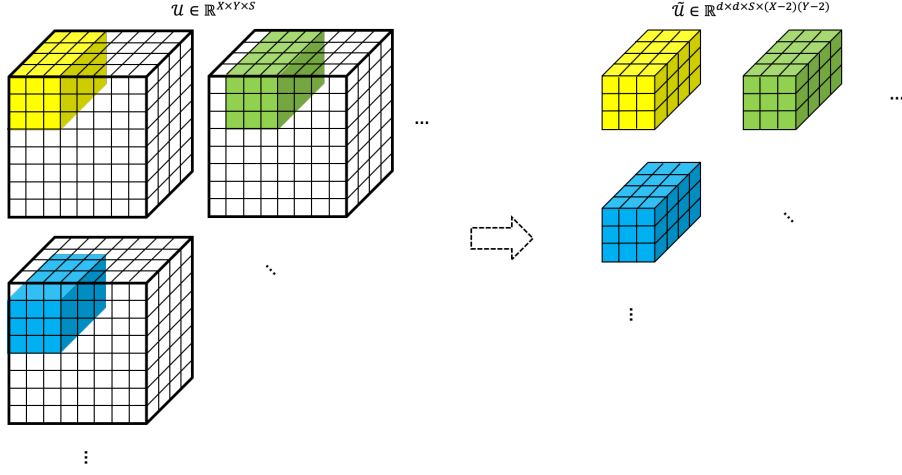


Figure 2. Visualization of Input Tensor Reshape

3.3. Backward Propagation of CPAC-Conv Layer

From the previous section, we have derived the tensor expression of CPAC-Conv layer shown as equation (10). Considering the simplest structure of a CNN model with CPAC-Conv layer (CPAC-CNN) used for classification as an example, the CPAC-CNN has one CPAC-Conv layer, and this layer is followed by one FC layer. So the output of the model could be expressed as equation (11).

$$\hat{y} = \mathcal{W}\tilde{\mathcal{V}} + b, \quad (11)$$

in which, $\hat{y} \in \mathbb{R}^C$, $\mathcal{W} \in \mathbb{R}^{(X-d+1)(Y-d+1) \times N \times C}$, $b \in \mathbb{R}^C$, and C is the number of class. The loss function is denoted as $\mathcal{L}(y, \hat{y})$, which represents the difference between the predicted labels \hat{y} and the real labels y . To estimate the unknown parameters in Neural Network, stochastic gradient descent and its variants are always applied by using back-propagation (Rumelhart et al., 1986). To update the parameters in CPAC-Conv layer, we need to start from deriving the gradient of the loss function $\mathcal{L}(y, \hat{y})$ w.r.t. the output \hat{y} , and then propagate the gradient backwards through each layer to derive the partial gradient w.r.t to each rank-one tensors in CPAC-Conv layer $(\frac{\partial \mathcal{L}}{\partial K_r^N}, \frac{\partial \mathcal{L}}{\partial K_r^X}, \frac{\partial \mathcal{L}}{\partial K_r^Y}, \frac{\partial \mathcal{L}}{\partial K_r^S})$.

3.3.1. Partial Derivative w.r.t. K_r^N

According to the chain rule, the expression of $\frac{\partial \mathcal{L}}{\partial K_r^N}$ is shown in equation (12), in which the first two components are the same as the original CNN models and we only need to derive $\frac{\partial \tilde{\mathcal{V}}}{\partial K_r^N}$.

$$\frac{\partial \mathcal{L}}{\partial K_r^N} = \frac{\partial \mathcal{L}}{\partial \hat{y}} \frac{\partial \hat{y}}{\partial \tilde{\mathcal{V}}} \frac{\partial \tilde{\mathcal{V}}}{\partial K_r^N} \quad (12)$$

At first, we calculate the differential of equation (10) at both sides w.r.t. K_r^N .

$$d\tilde{\mathcal{V}} = \left(\left(\left(\tilde{\mathcal{U}} \times_3 K_r^S \right) \times_2 K_r^Y \right) \times_1 K_r^X \right) \circ dK_r^N \quad (13)$$

After vectorizing both sides, we will have equation (14).

$$\text{vec}(d\tilde{\mathcal{V}}) = \text{vec} \left(\left(\left(\left(\tilde{\mathcal{U}} \times_3 K_r^S \right) \times_2 K_r^Y \right) \times_1 K_r^X \right) \circ dK_r^N \right) \quad (14)$$

We use $A_1 \in \mathbb{R}^{(X-d+1)(Y-d+1) \times 1}$ to denote the constant part $\left(\left(\left(\tilde{\mathcal{U}} \times_3 K_r^S \right) \times_2 K_r^Y \right) \times_1 K_r^X \right)$, and $dK_r^N \in \mathbb{R}^{N \times 1}$. Substituting A_1 into equation (14) yields.

$$\begin{aligned} \text{vec}(d\tilde{\mathcal{V}}) &= \text{vec} (A_1 \circ dK_r^N) \\ &= \text{vec} (A_1 [dK_r^N]^T) \\ &= (I_N \otimes A_1) \text{vec} ([dK_r^N]^T) \\ &= (I_N \otimes A_1) \text{vec}(dK_r^N) \\ \frac{\text{vec}(d\tilde{\mathcal{V}})}{\text{vec}(dK_r^N)} &= (I_N \otimes A_1) \\ \frac{\partial \tilde{\mathcal{V}}}{\partial K_r^N} &= I_N \otimes A_1^T \end{aligned} \quad (15)$$

In equation (15), because $dK_r^N \in \mathbb{R}^{N \times 1}$, we have $\text{vec}([dK_r^N]^T) = \text{vec}(dK_r^N)$.

3.3.2. Partial Derivative w.r.t. K_r^X

The expression of $\frac{\partial \mathcal{L}}{\partial K_r^X}$ is shown in equation (16), and we will derive $\frac{\partial \tilde{\mathcal{V}}}{\partial K_r^X}$.

$$\frac{\partial \mathcal{L}}{\partial K_r^X} = \frac{\partial \mathcal{L}}{\partial \hat{y}} \frac{\partial \hat{y}}{\partial \tilde{\mathcal{V}}} \frac{\partial \tilde{\mathcal{V}}}{\partial K_r^X} \quad (16)$$

At first, we calculate the differential of equation (10) at both sides w.r.t. K_r^X .

$$d\tilde{\mathcal{V}} = \left(\left(\left(\tilde{\mathcal{U}} \times_3 K_r^S \right) \times_2 K_r^Y \right) \times_1 dK_r^X \right) \circ K_r^N \quad (17)$$

After vectorizing both sides, we will have equation (18).

$$\text{vec}(d\tilde{\mathcal{V}}) = \text{vec} \left(\left(\left(\left(\tilde{\mathcal{U}} \times_3 K_r^S \right) \times_2 K_r^Y \right) \times_1 dK_r^X \right) \circ K_r^N \right) \quad (18)$$

We use $A_2 \in \mathbb{R}^{d \times (X-d+1)(Y-d+1)}$ to denote the constant part $\left(\left(\tilde{\mathcal{U}} \times_3 K_r^S \right) \times_2 K_r^Y \right)$, and $B_1 \in \mathbb{R}^{N \times 1}$ to denote the constant part K_r^N . After substituting A_2 and B_1 into equation (18), we can simplify it into equation (19).

$$\begin{aligned} \text{vec}(d\tilde{\mathcal{V}}) &= \text{vec} \left(A_2 \times_1 dK_r^X \circ B_1 \right) \\ &= \text{vec} \left(A_2^T dK_r^X B_1^T \right) \\ &= (B_1 \otimes A_2^T) \text{vec}(dK_r^X) \\ \frac{\text{vec}(d\tilde{\mathcal{V}})}{\text{vec}(dK_r^X)} &= (B_1 \otimes A_2^T) \\ \frac{\partial \tilde{\mathcal{V}}}{\partial K_r^X} &= B_1^T \otimes A_2 \end{aligned} \quad (19)$$

3.3.3. Partial Derivative w.r.t. K_r^Y

The expression of $\frac{\partial \mathcal{L}}{\partial K_r^Y}$ is shown in equation (20), and we will derive $\frac{\partial \tilde{\mathcal{V}}}{\partial K_r^Y}$.

$$\frac{\partial \mathcal{L}}{\partial K_r^Y} = \frac{\partial \mathcal{L}}{\partial \hat{y}} \frac{\partial \hat{y}}{\partial \tilde{\mathcal{V}}} \frac{\partial \tilde{\mathcal{V}}}{\partial K_r^Y} \quad (20)$$

At first, we calculate the differential of equation (10) at both sides w.r.t. K_r^Y .

$$d\tilde{\mathcal{V}} = \left(\left(\left(\tilde{\mathcal{U}} \times_3 K_r^S \right) \times_2 dK_r^Y \right) \times_1 K_r^X \right) \circ K_r^N \quad (21)$$

We use $\mathcal{A} \in \mathbb{R}^{d \times d \times (X-d+1)(Y-d+1)}$ to denote the constant part $(\tilde{\mathcal{U}} \times_3 K_r^S)$. After substituting it into equation (21), we can get the equation (22).

$$d\tilde{\mathcal{V}} = \left((\mathcal{A} \times_2 dK_r^Y) \times_1 K_r^X \right) \circ K_r^N \quad (22)$$

Then, we can use $\mathcal{A}_{(2)} \in \mathbb{R}^{d \times d \times (X-d+1)(Y-d+1)}$ to denote the mode-2 unfolding of \mathcal{A} . So that we can rewrite the inner part $(\mathcal{A} \times_2 dK_r^Y) \in \mathbb{R}^{d \times (X-d+1)(Y-d+1)}$ of equation (22) into $P((\mathcal{A}_{(2)})^T dK_r^Y) \in \mathbb{R}^{(X-d+1)(Y-d+1) \times d}$. $P(\cdot)$ represents a permutation operator, which means $(\mathcal{A}_{(2)})^T dK_r^Y$ and $\mathcal{A} \times_2 dK_r^Y$ are matrices containing the same elements, but arranged differently. Equation (22) can be transformed into equation (23).

$$d\tilde{\mathcal{V}} = [P((\mathcal{A}_{(2)})^T dK_r^Y) K_r^X] (K_r^N)^T \quad (23)$$

Further, we can use $B_2 \in \mathbb{R}^{d \times N}$ to denote $K_r^X (K_r^N)^T$. Substitute B_2 into equation (23) and vectorize both sides, we can get equation (24).

$$\begin{aligned} \text{vec}(d\tilde{\mathcal{V}}) &= \text{vec} \left(P((\mathcal{A}_{(2)})^T dK_r^Y) B_2 \right) \\ &= B_2^T \otimes I_{(X-d+1)(Y-d+1)} \text{vec} \left(P((\mathcal{A}_{(2)})^T dK_r^Y) \right) \end{aligned} \quad (24)$$

Because $P(\cdot)$ is a permutation operator, it is easy to show that $\text{vec}(P((\mathcal{A}_{(2)})^T dK_r^Y))$ is the same as $\text{vec}((\mathcal{A}_{(2)})^T dK_r^Y)$.

$$\begin{aligned}
\text{vec}(d\tilde{\mathcal{V}}) &= B_2^T \otimes I_{(X-d+1)(Y-d+1)} \text{vec}(P((\mathcal{A}_{(2)})^T dK_r^Y)) \\
&= B_2^T \otimes I_{(X-d+1)(Y-d+1)} \text{vec}((\mathcal{A}_{(2)})^T dK_r^Y) \\
&= (B_2^T \otimes I_{(X-d+1)(Y-d+1)})(I_1 \otimes \mathcal{A}_{(2)}^T) \text{vec}(dK_r^Y) \\
\frac{\text{vec}(d\tilde{\mathcal{V}})}{\text{vec}(dK_r^Y)} &= (B_2^T \otimes I_{(X-d+1)(Y-d+1)})(I_1 \otimes \mathcal{A}_{(2)}^T) \\
\frac{\partial \tilde{\mathcal{V}}}{\partial K_r^Y} &= [(B_2^T \otimes I_{(X-d+1)(Y-d+1)})(I_1 \otimes \mathcal{A}_{(2)}^T)]^T \\
&= (I_1 \otimes \mathcal{A}_{(2)})^T (B_2^T \otimes I_{(X-d+1)(Y-d+1)})^T \\
&= \mathcal{A}_{(2)}(B_2 \otimes I_{(X-d+1)(Y-d+1)})
\end{aligned} \tag{25}$$

3.3.4. Partial Derivative w.r.t. K_r^S

The expression of $\frac{\partial \mathcal{L}}{\partial K_r^S}$ is shown in equation (26), and we will derive $\frac{\partial \tilde{\mathcal{V}}}{\partial K_r^S}$.

$$\frac{\partial \mathcal{L}}{\partial K_r^S} = \frac{\partial \mathcal{L}}{\partial \hat{y}} \frac{\partial \hat{y}}{\partial \tilde{\mathcal{V}}} \frac{\partial \tilde{\mathcal{V}}}{\partial K_r^S} \tag{26}$$

At first, we calculate the differential of equation (10) at both sides w.r.t. K_r^S .

$$d\tilde{\mathcal{V}} = \left(\left(\left(\tilde{\mathcal{U}} \times_3 dK_r^S \right) \times_2 K_r^Y \right) \times_1 K_r^X \right) \circ K_r^N \tag{27}$$

In equation (27), we have $\mathcal{U} \in \mathbb{R}^{d \times d \times S \times (X-d+1)(Y-d+1)}$. We can use $\mathcal{U}_{(3)} \in \mathbb{R}^{S \times d^2 \times (X-d+1)(Y-d+1)}$ to represent the mode-3 unfolding of tensor \mathcal{U} . Similarly, we use $P(\cdot)$ to represent permutation operator and $(\mathcal{U}_{(3)}^T dK_r^S) \in \mathbb{R}^{d^2 \times (X-d+1)(Y-d+1)}$, $P(\mathcal{U}_{(3)}^T dK_r^S) \in \mathbb{R}^{d \times (X-d+1)(Y-d+1) \times d}$, $P(P(\mathcal{U}_{(3)}^T dK_r^S) K_r^Y) \in \mathbb{R}^{(X-d+1)(Y-d+1) \times d}$. So that $\left(\left(\tilde{\mathcal{U}} \times_3 dK_r^S \right) \times_2 K_r^Y \right) \in \mathbb{R}^{d \times (X-d+1)(Y-d+1)}$ in the equation (27) can be trans-

formed into equation $\left[P \left(P(\mathcal{U}_{(3)}^T dK_r^S) K_r^Y \right) \right]^T \in \mathbb{R}^{d \times (X-d+1)(Y-d+1)}$.

$$\begin{aligned} d\tilde{\mathcal{V}} &= \left(\left[P \left(P(\mathcal{U}_{(3)}^T dK_r^S) K_r^Y \right) \right]^T \times_1 K_r^X \right) \circ K_r^N \\ &= \left(P \left(P(\mathcal{U}_{(3)}^T dK_r^S) K_r^Y \right) K_r^X \right) (K_r^N)^T \end{aligned} \quad (28)$$

After vectorizing both sides in equation (28).

$$\begin{aligned} \text{vec}(d\tilde{\mathcal{V}}) &= \text{vec} \left(P \left(P(\mathcal{U}_{(3)}^T dK_r^S) K_r^Y \right) K_r^X (K_r^N)^T \right) \\ &= B_2^T \otimes I_{(X-d+1)(Y-d+1)} \text{vec} \left(P \left(P(\mathcal{U}_{(3)}^T dK_r^S) K_r^Y \right) \right) \\ &= B_2^T \otimes I_{(X-d+1)(Y-d+1)} \text{vec} \left(P(\mathcal{U}_{(3)}^T dK_r^S) K_r^Y \right) \\ &= (B_2^T \otimes I_{(X-d+1)(Y-d+1)}) ((K_r^Y)^T \otimes I_{d(X-d+1)(Y-d+1)}) \text{vec} \left(P(\mathcal{U}_{(3)}^T dK_r^S) \right) \\ &= (B_2^T \otimes I_{(X-d+1)(Y-d+1)}) ((K_r^Y)^T \otimes I_{d(X-d+1)(Y-d+1)}) \text{vec} \left(\mathcal{U}_{(3)}^T dK_r^S \right) \\ &= (B_2^T \otimes I_{(X-d+1)(Y-d+1)}) ((K_r^Y)^T \otimes I_{d(X-d+1)(Y-d+1)}) \left(I_1 \otimes \mathcal{U}_{(3)}^T \right) \text{vec} \left(dK_r^S \right) \\ \frac{\text{vec}(d\tilde{\mathcal{V}})}{\text{vec}(dK_r^S)} &= (B_2^T \otimes I_{(X-d+1)(Y-d+1)}) ((K_r^Y)^T \otimes I_{d(X-d+1)(Y-d+1)}) \left(I_1 \otimes \mathcal{U}_{(3)}^T \right) \\ \frac{\partial \tilde{\mathcal{V}}}{\partial K_r^S} &= \left[(B_2^T \otimes I_{(X-d+1)(Y-d+1)}) ((K_r^Y)^T \otimes I_{d(X-d+1)(Y-d+1)}) \mathcal{U}_{(3)}^T \right]^T \\ \frac{\partial \tilde{\mathcal{V}}}{\partial K_r^S} &= \mathcal{U}_{(3)} (K_r^Y \otimes I_{d(X-d+1)(Y-d+1)}) (B_2 \otimes I_{(X-d+1)(Y-d+1)}) \end{aligned} \quad (29)$$

Combining equations (15,19,25,29), we generated the detailed expressions of $\left\{ \frac{\partial \tilde{\mathcal{V}}}{\partial K_r^N}, \frac{\partial \tilde{\mathcal{V}}}{\partial K_r^X}, \frac{\partial \tilde{\mathcal{V}}}{\partial K_r^Y}, \frac{\partial \tilde{\mathcal{V}}}{\partial K_r^S} \right\}$, which will be used to update decomposed kernels of CPAC-Conv layer in the backward propagation.

Up to now, we have finished deriving the forward and backward propagations of CPAC-Conv layer, which makes CPAC-Conv layer well-prepared to replace the original convolutional layer, and in the following section 4, we will give a general setup of Convolutional Neural Network with CPAC-Conv layer (CPAC-CNN) and analyze the compression effect.

Table 1. CPAC-CNN Setup and Notations

Layer Index	Layer Name	Weights (Rank)	Input (Shape)	Output
1	CPAC-Conv	$K_r^{(1)X}, K_r^{(1)Y}, K_r^{(1)S}, K_r^{(1)N_1}$ ($r = 1, \dots, R$)	$\tilde{\mathcal{U}}^{(1)}$ ($\mathbb{R}^{d \times d \times S \times (X-(d-1))(Y-(d-1))}$)	$\tilde{\mathcal{V}}^{(1)}$ ($\mathbb{R}^{(X-(d-1))(Y-(d-1)) \times N_1}$)
2, ..., L - 1	CPAC-Conv	$K_r^{(l)X}, K_r^{(l)Y}, K_r^{(l)N_{l-1}}, K_r^{(l)N_l}$ ($r = 1, \dots, R$)	$\tilde{\mathcal{U}}^{(l)}$ ($\mathbb{R}^{d \times d \times N_{l-1} \times (X-l(d-1))(Y-l(d-1))}$)	$\tilde{\mathcal{V}}^{(l)}$ ($\mathbb{R}^{(X-l(d-1))(Y-l(d-1)) \times N_l}$)
L	FC	$\mathcal{W}^{(L)}, b$	$\tilde{\mathcal{U}}^{(L)}$ ($\mathbb{R}^{(X-(L-1)(d-1))(Y-(L-1)(d-1)) \times N_{L-1}}$)	\hat{y} (\mathbb{R}^C)

4. Convolutional Neural Network with CPAC-Conv Layer (CPAC-CNN)

In this section, we will give a general setup of convolutional neural network with one or more CPAC-Conv layers and analyze the effect of model compression. It is worth noting that the proposed CPAC-Conv layer is extendable to other deep learning models.

Suppose the CPAC-CNN consists of L layers, among them, the first $(L - 1)$ layers are CPAC-Conv layers, and the L_{th} layer (output layer) is a fully-connected (FC) layer. Similar to section 3.2, we use $\tilde{\mathcal{U}}^{(l)}$ and $\tilde{\mathcal{V}}^{(l)}$ to represent the input and output of the l_{th} layer, in which $\tilde{\mathcal{U}}^{(l)} \in \mathbb{R}^{d \times d \times N_{l-1} \times (X-l(d-1))(Y-l(d-1))}$, $\tilde{\mathcal{V}}^{(l)} \in \mathbb{R}^{(X-l(d-1))(Y-l(d-1)) \times N_l}$, $l = 1, \dots, L - 1$. The detailed model setup and notations can be found in Table 1.

Given the general CPAC-CNN setup with $(L - 1)$ CPAC-Conv layers and one FC layer, we further summarize the back-propagation expressions of CPAC-CNN according to the derivations in section 3.3. For an arbitrary l_{th} ($l = 1, \dots, L - 1$) CPAC-Conv layer, the gradients of the loss function w.r.t. the weight matrices are computed as equations (30).

$$\begin{aligned}
\frac{\partial \mathcal{L}}{\partial K_r^{(l)X}} &= \frac{\partial \mathcal{L}}{\partial \tilde{\mathcal{V}}^{(l)}} \frac{\partial \tilde{\mathcal{V}}^{(l)}}{\partial K_r^X}, r = 1, \dots, R \\
\frac{\partial \mathcal{L}}{\partial K_r^{(l)Y}} &= \frac{\partial \mathcal{L}}{\partial \tilde{\mathcal{V}}^{(l)}} \frac{\partial \tilde{\mathcal{V}}^{(l)}}{\partial K_r^Y}, r = 1, \dots, R \\
\frac{\partial \mathcal{L}}{\partial K_r^{(l)N_{l-1}}} &= \frac{\partial \mathcal{L}}{\partial \tilde{\mathcal{V}}^{(l)}} \frac{\partial \tilde{\mathcal{V}}^{(l)}}{\partial K_r^{(l)N_{l-1}}}, r = 1, \dots, R \\
\frac{\partial \mathcal{L}}{\partial K_r^{(l)N_l}} &= \frac{\partial \mathcal{L}}{\partial \tilde{\mathcal{V}}^{(l)}} \frac{\partial \tilde{\mathcal{V}}^{(l)}}{\partial K_r^{(l)N_l}}, r = 1, \dots, R
\end{aligned} \tag{30}$$

In equations (30), the $\frac{\partial \mathcal{L}}{\partial \tilde{\mathcal{V}}^{(l)}}$ is the gradient of the loss function w.r.t. the output of

l_{th} , which is back propagated from the $(l + 1)_{th}$ layer, and the detailed expressions of $\left\{ \frac{\partial \tilde{y}^{(l)}}{\partial K_r^{(l)X}}, \frac{\partial \tilde{y}^{(l)}}{\partial K_r^{(l)Y}}, \frac{\partial \tilde{y}^{(l)}}{\partial K_r^{(l)N_{l-1}}}, \frac{\partial \tilde{y}^{(l)}}{\partial K_r^{(l)N_l}} \right\}$ are in equations (19,25,29,15). Thus, we could summarize the training process of CPAC-CNN as Algorithm 1. Note that for simplicity, we exclude the activation function and suppose the rank R are selected to be same for all layers $1, \dots, L - 1$. Compared with original CNN, one important property of our proposed CPAC-CNN is it could reduce the model parameters by setting different values of rank R in CP-decomposition. For example, given a convolutional layer with kernel $\mathcal{K} \in \mathbb{R}^{d \times d \times S \times N}$, the number of parameters in this layer is $M_1 = d \times d \times S \times N$. In our proposed CPAC-Conv layer, we will use a series of small kernels $K_r^X, K_r^Y, K_r^S, K_r^{N_l} (r = 1, \dots, R)$ to approximate the original kernel. The number of parameters in these kernels is $M_2 = R \times (d + d + S + N)$. To numerically analyze the compression effect of CPAC-Conv layer, we use compression ratio (CR) to denote the ratio of parameters in CPAC-Conv layers and Conv layers, which is expressed as $CR = \frac{M_2}{M_1}$. It is easy to see that M_2 is determined by the rank R of CP-decomposition, and there always exists an R which makes $M_2 < M_1$. By controlling the value of R , our proposed CPAC-Conv layer could use fewer parameters to approximate convolutional layer to reduce the model complexity. The proposed CPAC-Conv layer can also be extended and integrated with other deep learning models.

Algorithm 1 Forward and Backward-Propagation for CPAC-CNN

1: **Inputs:**

$$\mathcal{U} \in \mathbb{R}^{X \times Y \times S}, y$$

2: **Initialize:**

$$K_r^{(l)X}, K_r^{(l)Y}, K_r^{(l)N_{l-1}}, K_r^{(l)N_l} (N_0 = S; r = 1, \dots, R; l = 1, \dots, L - 1)$$

$$\tilde{\mathcal{W}}^{(L)}, b$$

$$\tilde{\mathcal{U}}^{(1)} \leftarrow \text{reshape the input } \mathcal{U}$$

3: **Forward Propagation:**

4: **for** $l = 1$ to $L - 1$ **do**

5: $\tilde{\mathcal{V}}^{(l)} \leftarrow \sum_{r=1}^R \left(\left(\left(\tilde{\mathcal{U}}^{(l)} \times_3 K_r^{(l)N_{l-1}} \right) \times_2 K_r^{(l)Y} \right) \times_1 K_r^{(l)X} \right) \circ K_r^{(l)N_l}$

6: **if** $l \leq L - 2$ **then**

7: $\tilde{\mathcal{U}}^{(l+1)} \leftarrow \text{reshape the } \tilde{\mathcal{V}}^{(l)}$

8: **end if**

9: **end for**

10: Output of Fully Connected layer $\hat{y} = \mathcal{W}^{(L)} \tilde{\mathcal{V}}^{(L-1)} + b$

11: Calculate loss function $\mathcal{L}(y, \hat{y})$

12: **Backward Propagation:**

13: Calculate $\left\{ \frac{\partial \mathcal{L}}{\partial \hat{y}}, \frac{\partial \hat{y}}{\partial \mathcal{V}^{(L-1)}}, \frac{\partial \hat{y}}{\partial \mathcal{W}^{(L)}} \right\}$ ▷ the same as original CNN

14: Update $\tilde{\mathcal{W}}^{(L)}$

15: **for** $l = L - 1$ to 1 **do**

16: **for** $r = 1$ to R **do**

17: Calculate $\left\{ \frac{\partial \tilde{\mathcal{V}}^{(l)}}{\partial K_r^{(l)X}}, \frac{\partial \tilde{\mathcal{V}}^{(l)}}{\partial K_r^{(l)Y}}, \frac{\partial \tilde{\mathcal{V}}^{(l)}}{\partial K_r^{(l)N_{l-1}}}, \frac{\partial \tilde{\mathcal{V}}^{(l)}}{\partial K_r^{(l)N_l}} \right\}$ ▷ equations (19,25,29,15)

18: Update $K_r^{(l)X}, K_r^{(l)Y}, K_r^{(l)N_{l-1}}, K_r^{(l)N_l}$ ▷ according to selected optimizer

19: **end for**

20: **end for**

5. Case Study

In this section, we apply our proposed CPAC-CNN model on two datasets for method validation, one of which is classification on the MNIST dataset (LeCun and Cortes, 2010), and the other is defect diagnosis on the Magnetic Tile Defects dataset (Huang et al., 2018). By comparing with the original CNN model, we would like to justify the

strengths of our proposed method into two aspects: 1) our proposed CPAC-Conv layer could receive a comparable performance compared with original Convolutional layer by using fewer parameters; 2) the CPAC-Conv layer increases the interpretability of the output feature maps. The experiments are implemented by PyTorch (Paszke et al., 2019) on a single NVIDIA GeForce GTX 1080Ti GPU. The code will be available on <https://github.com/wyn430/CPAC-CNN> upon paper submission.

5.1. Case 1: MNIST Dataset

The MNIST dataset is originally collected for handwritten digit recognition, and we use it to test the performance of our model on classification task. This dataset consists of 60000 28×28 grayscale images for training, and 10000 for testing. We use CPAC-CNN with one CPAC-Conv layer and two CPAC-Conv layers to compare with CNN with one Conv layer and two Conv layers, respectively. The hyper-parameter in our proposed CPAC-CNN is the rank R of CP-Decomposition, which will change the the number of trainable parameters in the model. In Table 2, we summarize the experiment results and model information, which include model structure, rank R of CP-Decomposition, kernel size of convolution operation, number of parameters in Conv/CPAC-Conv layers, compression ratio (CR), and classification accuracy. From Table 2, we can see that 1) with the increase of Rank (R), the CPAC-CNN tends to have more parameters, and receive a better classification accuracy; 2) compare the performance of CNN and CPAC-CNN, we can always find a R to let CPAC-CNN receive a comparable classification performance with fewer parameters.

For better visualization, we show the change of classification accuracy and loss along with various values of rank in Figure 3. The left plot in Figure 3 is the result of single-layer models and the right plot is the result of double-layer models. The blue dashed line in Figure 3 represents the classification accuracy of CNN, and the red dotted line represents the loss function value of CNN. The blue line with triangle markers represents the change of classification accuracy of CPAC-CNN with various ranks, and the red line with star markers represents the change of loss function value of CPAC-CNN with various ranks. The horizontal axis represents different ranks, the left vertical axis represents classification accuracy, and the right vertical axis represents the value of

Table 2. Experiment Results on MNIST

Model	Structure	Rank (R)	Kernel Size	# of Parameters	CR*	Accuracy			
CNN	1×Conv Layer 1×FC Layer	-	(8, 3, 3, 1)	72	1	0.9794			
		1			0.2083	0.9518			
		2	(8, R)		0.4167	0.9669			
		3	(3, R)		0.6250	0.9677			
		4	(3, R)		0.8333	0.9773			
		5	(1, R)		1.0417	0.9782			
CPAC-CNN	1×CPAC-Conv Layer 1×FC Layer	6		15 R	1.2500	0.9782			
		<hr/>							
		CNN	2×Conv Layer 1×FC Layer		-	(8, 3, 3, 1), (8, 3, 3, 8)	648	1	0.9844
					1			0.0571	0.9278
					2			0.1142	0.9679
					3			0.1713	0.9774
4				0.2284	0.9788				
5	(8, R), (8, R)			0.2855	0.9805				
CPAC-CNN	2×CPAC-Conv Layer 1×FC Layer	6	(3, R), (3, R)	37 R	0.3426	0.9767			
		7	(3, R), (3, R)		0.3997	0.9801			
		8	(1, R), (8, R)		0.4568	0.9800			
		9			0.5139	0.9830			
		10			0.5710	0.9833			
		11			0.6281	0.9815			
		12			0.6852	0.9842			

*CR: Compression Ratio

loss function. The general patterns in Figure 3 show that with a larger rank (R) the CPAC-CNN receives better performance and gradually approaches the corresponding CNN. Considering the results shown in Table 2 and Figure 3, we can conclude that 1) compared with original CNN, our proposed CPAC-CNN could receive a comparable classification accuracy with fewer parameters; 2) the classification accuracy and loss value tend to improve with the increasing of rank R and rank R determines the number of parameters in CPAC-CNN, which means we can tune the rank R to meet the accuracy requirement and satisfy the computation resource limitation; 3) the compression effect will be more significant as the model containing more CPAC-Conv layers.

5.2. Case 2: Magnetic Tile Defects Dataset

The Magnetic Tile Defects data are collected for defects detection and diagnosis in the magnetic tile automation process. The samples are shown in Figure 4. In this dataset, it contains six classes consisting of five types of defects (blowhole, crack, break, fray, uneven) and one defect-free class. Because it is an unbalanced dataset and there are too few samples belonging to crack and fray, we apply the data augmentation technique, such as flip and rotate, to enrich the dataset. Furthermore, because the samples in the

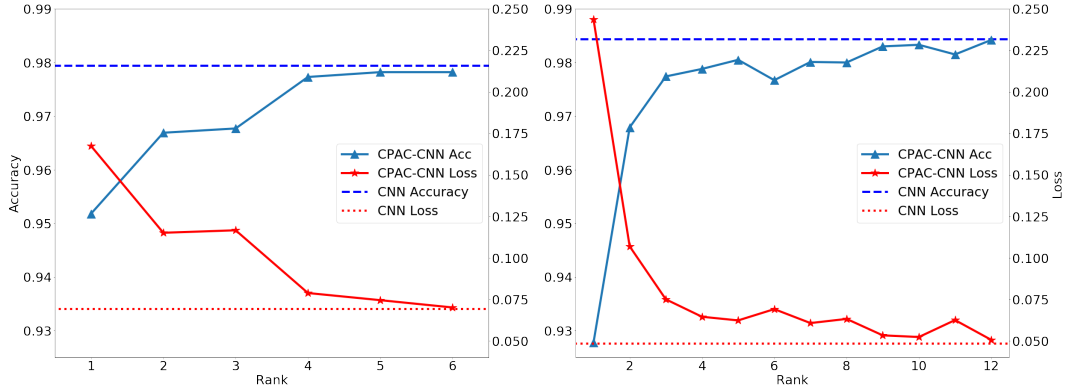


Figure 3. Performance Comparison Between CNN and CPAC-CNN on MNIST, **Left:** one Conv/CPAC-Conv Layer, **Right:** two Conv/CPAC-Conv Layers

dataset do not have the same shape, we resize all the image data into 100×100 . Finally, as we want to test the model performance on defect diagnosis, we use the dataset containing 563 100×100 binary samples for training and 100 samples for testing. Similarly, we test the performances of single-layer and double-layer CPAC-CNN and compare them with the corresponding CNN model. The detailed experiment settings and results are summarized in Table 3, from which we can see that the number of parameters in CPAC-CNN is controlled by rank (R) and it will be comparable to the corresponding CNN with fewer parameters.

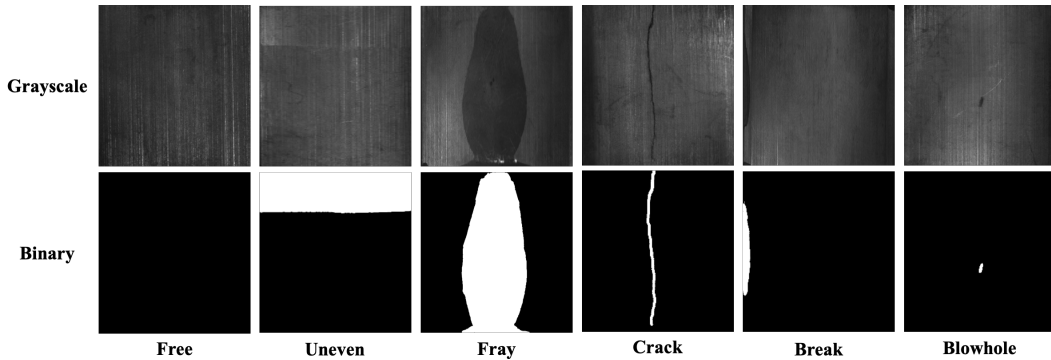


Figure 4. Image Data of Magnetic Tile Defect

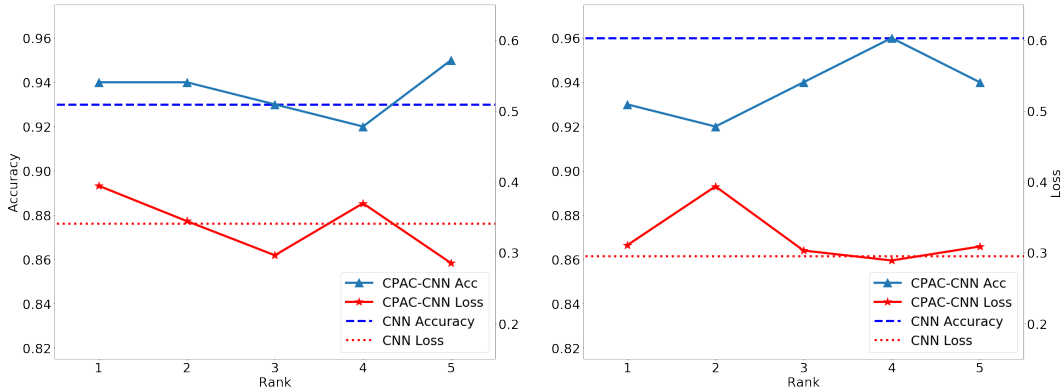
The visualization of performance comparison on defects diagnosis are shown in Figure 5. Similarly, the left plot shows the comparison between single-layer models while the right plot shows the comparison between double-layer models. In Figure 5, we can see that the classification accuracy of CPAC-CNN (blue lines with triangle markers) is comparable to CNN (blue dashed lines), and the value of loss function in CPAC-CNN

Table 3. Experiment Results on Magnetic Tile Defects

Model	Structure	Rank (R)	Kernel Size	# of Parameters	CR*	Accuracy
CNN	1×Conv Layer 1×FC Layer	-	(8, 3, 3, 1)	72	1	0.93
		1	(8, R)		0.2083	0.94
CPAC-CNN	1×CPAC-Conv Layer 1×FC Layer	2	(3, R)	15R	0.4167	0.94
		3	(3, R)		0.6250	0.93
		4	(3, R)		0.8333	0.92
		5	(1, R)		1.0417	0.95
CNN	2×Conv Layer 2×FC Layer	-	(8, 3, 3, 1), (8, 3, 3, 8)	648	1	0.96
		1	(8, R), (8, R)		0.0571	0.93
CPAC-CNN	2×CPAC-Conv Layer 2×FC Layer	2	(3, R), (3, R)	37R	0.1142	0.92
		3	(3, R), (3, R)		0.1713	0.94
		4	(3, R), (3, R)		0.2284	0.96
		5	(1, R), (8, R)		0.2855	0.94

*CR: Compression Ratio

(red lines with star markers) also approaches CNN (rad dotted lines). Besides aforementioned conclusions, we can find out the proposed CPAC-Conv layer can realize significant compression performance when the defects dataset has fewer samples and less classes compared with MNIST. Specifically, we can use around 23% parameters compared with conventional CNN to receive the same 96% testing accuracy. The original design of CNN have redundancy in parameters and our proposed method provides a reasonable and flexible way to control the model complexity according to different tasks and could compress the model to reduce the parameter redundancy.

**Figure 5.** Performance Comparison Between CNN and CPAC-CNN on Magnetic Tile Defect, **Left:** one Conv/CPAC-Conv Layer, **Right:** two Conv/CPAC-Conv Layers

5.3. Interpretation of Feature Map

From the results shown in sections 5.1 and 5.2, we can conclude that the rank of CP-decomposition determines the number of parameters in the CPAC-Conv layer and further influence the model performance. As we discussed before, the CPAC-Conv layer serves as a feature extractor in CPAC-CNN. In this section, we will further illustrate how our proposed method influences the extracted features.

We use the single-layer CPAC-CNN as the example, which consists of one CPAC-Conv layer as the feature extractor and one FC layer as the classifier. According to equation (10), we will decompose the original convolutional kernel \mathcal{K} into R groups of small kernels $K_r^S, K_r^X, K_r^Y, K_r^N, (r = 1, \dots, R)$, and then sum up the features extracted by each kernel group as the output feature map for further classification. To show the relationship between extracted features and kernels, we plot the overall feature map and features from each specific kernel group in Figures 6 and 7.

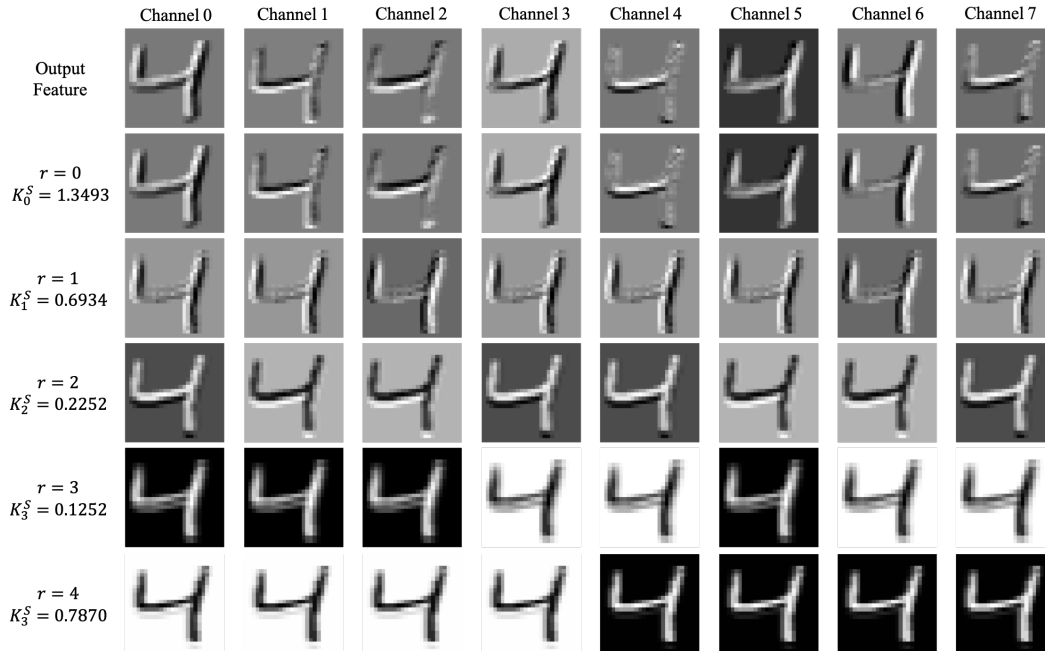


Figure 6. Relationship Between Features and Kernels on MNIST Data

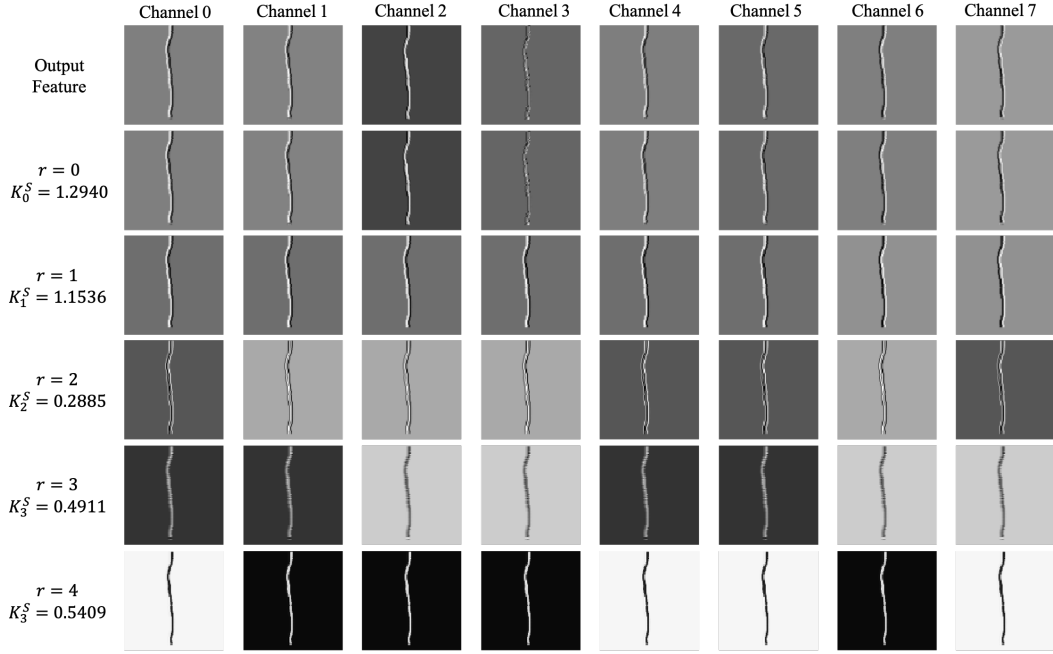


Figure 7. Relationship Between Features and Kernels on Defect Data

We plot the feature maps from single-layer CPAC-CNN and set the rank $R = 5$ according to the results in Tables 2 and 3 so that our proposed CPAC-CNN contains 5 kernel groups. There are 6 rows and 8 columns in both Figures 6 and 7. Each column represents one channel of the output feature maps, the first row represents the overall output feature maps, and each of the rest 5 rows represents features extracted from the corresponding kernel group. By analyzing these two figures, we can find out that the features extracted from the kernel group with the largest K_r^S share almost the same pattern as the overall output feature. If we consider the kernel groups as a set of basis decomposed from the original convolutional kernel, one with the largest K_r^S can be regarded as the most significant basis and output the most informative features. In this perspective, the value of K_r^S could represent the significance of corresponding features, and if we use the CPAC-Conv layer as the feature extractor, we could select the most significant kernel group to get the most informative feature to further reduce the computation cost and improve model efficiency.

6. Conclusion

With all the theoretical derivation and analysis in the case study, we proposed the CPAC-Conv layer and further built the CPAC-CNN to compress the original CNN model without decaying the performance. In our proposed CPAC-Conv layer, we decompose the convolutional kernel into R kernel groups and derive the complete expressions of its forward and backward propagations. With the help of CP-decomposition, we could approximate the original convolution operation with fewer parameters, which reduces the model redundancy and computation cost. And then, we propose the general setup of the CPAC-CNN model along with its training algorithm. In this way, we could stack multiple CPAC-Conv layers and use it with other types of layers to build neural networks for various tasks. Finally, as a feature extractor, we find out the value of K_r^S indicates the significance of the feature map output from this kernel group, which could help us to interpret the importance of output features and provide us an indicator in feature selection.

In future work, we could extend the CPAC-Conv layer to serve as the feature extraction module in other deep learning models and other applications, such as process monitoring, image segmentation, quality improvement, etc. The indicator of feature significance could further be used in feature selection and combine with active learning to make the model training more efficient. Finally, tensor decomposition techniques can be adapted to other types of layers (i.e. LSTM (Hochreiter and Schmidhuber, 1997)) in Neural Network.

References

- G. G. Calvi, A. Moniri, M. Mahfouz, Z. Yu, Q. Zhao, and D. P. Mandic. Tucker Tensor Layer in Fully Connected Neural Networks. 2019. URL <http://arxiv.org/abs/1903.06133>.
- M. Crowder, J. R. Magnus, and H. Neudecker. *Matrix Differential Calculus with Applications in Statistics and Econometrics.*, volume 152. 1989. ISBN 9781119541202. .
- P. L. Fackler. Notes on Matrix Calculus. pages 1–14, 2005.
- Z. Gao, W. Guo, and X. Yue. Optimal integration of supervised tensor decomposition and ensemble learning for itin situ quality evaluation in friction stir blind riveting. *IEEE Trans-*

- actions on Automation Science and Engineering*, 2020.
- P. Geladi. Some special topics in multivariate image analysis. *Chemometrics and Intelligent Laboratory Systems*, 14(1):375 – 390, 1992. ISSN 0169-7439. . URL <http://www.sciencedirect.com/science/article/pii/0169743992801190>. Proceedings of the 2nd Scandinavian Symposium on Chemometrics.
- R. Girshick. Fast r-cnn. In *2015 IEEE International Conference on Computer Vision (ICCV)*, pages 1440–1448, 2015.
- K. He, X. Zhang, S. Ren, and J. Sun. Deep residual learning for image recognition. In *2016 IEEE Conference on Computer Vision and Pattern Recognition (CVPR)*, pages 770–778, 2016.
- S. Hochreiter and J. Schmidhuber. Long short-term memory. *Neural Computation*, 9(8): 1735–1780, 1997.
- Y. Huang, C. Qiu, Y. Guo, X. Wang, and K. Yuan. Surface Defect Saliency of Magnetic Tile. *IEEE International Conference on Automation Science and Engineering*, 2018-August (June):612–617, 2018. ISSN 21618089. .
- J. Jin and J. Shi. Feature-preserving data compression of stamping tonnage information using wavelets. *Technometrics*, 41(4):327–339, 1999. . URL <https://www.tandfonline.com/doi/abs/10.1080/00401706.1999.10485932>.
- H. A. L. Kiers. Towards a standardized notation and terminology in multiway analysis. *Journal of Chemometrics*, 14(3):105–122, 2000. .
- T. G. Kolda and B. W. Bader. Tensor decompositions and applications. *SIAM review*, 51(3): 455–500, 2009.
- A. Krizhevsky, I. Sutskever, and G. E. Hinton. Imagenet classification with deep convolutional neural networks. In F. Pereira, C. J. C. Burges, L. Bottou, and K. Q. Weinberger, editors, *Advances in Neural Information Processing Systems 25*, pages 1097–1105. Curran Associates, Inc., 2012. URL <http://papers.nips.cc/paper/4824-imagenet-classification-with-deep-convolutional-neural-networks.pdf>.
- V. Lebedev, Y. Ganin, M. Rakhuba, I. Oseledets, and V. Lempitsky. Speeding-up convolutional neural networks using fine-tuned CP-decomposition. *3rd International Conference on Learning Representations, ICLR 2015 - Conference Track Proceedings*, pages 1–11, 2015.
- Y. LeCun and C. Cortes. MNIST handwritten digit database. 2010. URL <http://yann.lecun.com/exdb/mnist/>.
- Y. Li, H. Sun, X. Deng, C. Zhang, H.-P. B. Wang, and R. Jin. Manufacturing quality prediction

- using smooth spatial variable selection estimator with applications in aerosol jet printed electronics manufacturing. *IISE Transactions*, 52(3):321–333, 2020. . URL <https://doi.org/10.1080/24725854.2019.1593556>.
- C. Liu, A. Law, D. Roberson, and Z. Kong. Image analysis-based closed loop quality control for additive manufacturing with fused filament fabrication. *Journal of Manufacturing Systems*, 51:86, 04 2019. .
- H. Lu, K. N. Plataniotis, and A. N. Venetsanopoulos. Mpca: Multilinear principal component analysis of tensor objects. *IEEE Transactions on Neural Networks*, 19(1):18–39, 2008.
- J. R. Magnus and H. Neudecker. Matrix differential calculus with applications to simple, hadamard, and kronecker products. *Journal of Mathematical Psychology*, 29(4):474 – 492, 1985. ISSN 0022-2496. . URL <http://www.sciencedirect.com/science/article/pii/0022249685900069>.
- S. G. Mallat. Multifrequency channel decompositions of images and wavelet models. *IEEE Transactions on Acoustics, Speech, and Signal Processing*, 37(12):2091–2110, 1989.
- J. Masci, U. Meier, D. C. Ciresan, and J. Schmidhuber. Stacked convolutional auto-encoders for hierarchical feature extraction. In *ICANN*, 2011.
- P. Nomikos and J. MacGregor. Monitoring batch processes using multiway principal component analysis. *AIChE Journal*, 40(8):1361–1375, 1994. .
- A. Novikov, D. Podoprikin, A. Osokin, and D. Vetrov. Tensorizing neural networks. *Advances in Neural Information Processing Systems*, 2015-Janua:442–450, 2015. ISSN 10495258.
- E. E. Papalexakis, C. Faloutsos, and N. D. Sidiropoulos. Tensors for data mining and data fusion: Models, applications, and scalable algorithms. *ACM Transactions on Intelligent Systems and Technology (TIST)*, 8(2):1–44, 2016.
- A. Paszke, S. Gross, F. Massa, A. Lerer, J. Bradbury, G. Chanan, T. Killeen, Z. Lin, N. Gimeshein, L. Antiga, A. Desmaison, A. Kopf, E. Yang, Z. DeVito, M. Raison, A. Tejani, S. Chilamkurthy, B. Steiner, L. Fang, J. Bai, and S. Chintala. Pytorch: An imperative style, high-performance deep learning library. In H. Wallach, H. Larochelle, A. Beygelzimer, F. dAlché Buc, E. Fox, and R. Garnett, editors, *Advances in Neural Information Processing Systems 32*, pages 8026–8037. Curran Associates, Inc., 2019. URL <http://papers.nips.cc/paper/9015-pytorch-an-imperative-style-high-performance-deep-learning-library.pdf>.
- K. Paynabar and J. Jin. Characterization of non-linear profiles variations using mixed-effect

- models and wavelets. *Iie transactions*, 43(4):275–290, 2011.
- D. E. Rumelhart, G. E. Hinton, and R. J. Williams. Learning Representations by Back-propagating Errors. *Nature*, 323(6088):533–536, 1986. . URL <http://www.nature.com/articles/323533a0>.
- N. Sergin and H. Yan. High-dimensional Nonlinear Profile Monitoring based on Deep Probabilistic Autoencoders. pages 1–23, 2019. URL <http://arxiv.org/abs/1911.00482>.
- C. Shao, J. J. Jin, and S. Jack Hu. Dynamic sampling design for characterizing spatiotemporal processes in manufacturing. *Journal of Manufacturing Science and Engineering*, 139(10), 2017.
- K. Simonyan and A. Zisserman. Very deep convolutional networks for large-scale image recognition. In *International Conference on Learning Representations*, 2015.
- L. R. Tucker. Some mathematical notes on three-mode factor analysis. *Psychometrika*, 31: 279–311, 1966c.
- M. A. O. Vasilescu and D. Terzopoulos. Multilinear image analysis for facial recognition. *Object recognition supported by user interaction for service robots*, 2:511–514 vol.2, 2002.
- H. Yan, K. Paynabar, and J. Shi. Anomaly detection in images with smooth background via smooth-sparse decomposition. *Technometrics*, 59(1):102–114, 2017. . URL <https://doi.org/10.1080/00401706.2015.1102764>.
- J. Ye, R. Janardan, and Q. Li. GPCA: An efficient dimension reduction scheme for image compression and retrieval. *KDD-2004 - Proceedings of the Tenth ACM SIGKDD International Conference on Knowledge Discovery and Data Mining*, pages 354–363, 2004.
- X. Yue. Data decomposition for analytics of engineering systems: Literature review, methodology formulation, and future trends. In *International Manufacturing Science and Engineering Conference*, volume 58745, page V001T02A011. American Society of Mechanical Engineers, 2019.
- X. Yue, H. Yan, J. G. Park, Z. Liang, and J. Shi. A wavelet-based penalized mixed-effects decomposition for multichannel profile detection of in-line raman spectroscopy. *IEEE Transactions on Automation Science and Engineering*, 15(3):1258–1271, 2018.
- X. Yue, J. G. Park, Z. Liang, and J. Shi. Tensor mixed effects model with application to nanomanufacturing inspection. *Technometrics*, 62(1):116–129, 2020.